Biochemical and structural characterization of a class A β-lactamase from Nocardia cyriacigeorgica

Jérôme Feuillard, Julie Couston, Yvonne Benito, Elisabeth Hodille, Oana Dumitrescu, Mickaël Blaise

STRUCTURAL BIOLOGY COMMUNICATIONS

ISSN 2053-230X

Received 2 October 2023
Accepted 13 December 2023

Edited by M. W. Bowler, European Molecular Biology Laboratory, France

‡ These authors contributed equally to this work.

Keywords: *Nocardia*; class A β-lactamases; β-lactam resistance; antibiotic resistance; β-lactams.

PDB reference: class A β-lactamase from *Nocardia cyriacigeorgica*, 8qnn

Supporting information: this article has supporting information at journals.iucr.org/f

Biochemical and structural characterization of a class A β-lactamase from *Nocardia cyriacigeorgica*

Jérôme Feuillard,[a]‡ Julie Couston,[a]‡ Yvonne Benito,[b] Elisabeth Hodille,[b,c] Oana Dumitrescu[b,c] and Mickaël Blaise[a]*

[a]IRIM, Montpellier University, CNRS, Montpellier, France, [b]Institut des Agents Infectieux, Hospices Civils de Lyon, Hôpital de la Croix-Rousse, Centre de Biologie Nord, Lyon, France, and [c]Centre International de Recherche en Infectiologie (CIRI), INSERM U1111, CNRS UMR5308, ENS Lyon, Université Lyon 1, Lyon, France. *Correspondence e-mail: mickael.blaise@irim.cnrs.fr

Nocardia are Gram-positive bacteria from the Actinobacteria phylum. Some *Nocardia* species can infect humans and are usually considered to be opportunist pathogens, as they often infect immunocompromised patients. Although their clinical incidence is low, many *Nocardia* species are now considered to be emerging pathogens. Primary sites of infection by *Nocardia* are the skin or the lungs, but dissemination to other body parts is very frequent. These disseminated infections are very difficult to treat and thus are tackled with multiple classes of antibiotics, in addition to the traditional treatment targeting the folate pathway. β-Lactams are often included in the regimen, but many *Nocardia* species present moderate or strong resistance to some members of this drug class. Genomic, microbiological and biochemical studies have reported the presence of class A β-lactamases (ABLs) in a handful of *Nocardia* species, but no structural investigation of *Nocardia* β-lactamases has yet been performed. In this study, the expression, purification and preliminary biochemical characterization of an ABL from an *N. cyriacigeorgica* (NCY-1) clinical strain are reported. The crystallization and the very high resolution crystal structure of NCY-1 are also described. The sequence and structural analysis of the protein demonstrate that NCY-1 belongs to the class A1 β-lactamases and show its very high conservation with ABLs from other human-pathogenic *Nocardia*. In addition, the presence of one molecule of citrate tightly bound in the catalytic site of the enzyme is described. This structure may provide a solid basis for future drug development to specifically target *Nocardia* spp. β-lactamases.

1. Introduction

Nocardiosis is an infectious disease caused by environmental bacteria from the *Nocardia* genus. *Nocardia* are Gram-positive bacteria from the Actinomycetota (or Actinobacteria) phylum. To date, about 130 species of *Nocardia* have been reported (https://www.bacterio.net/genus/nocardia), of which about 40 species are human pathogens and clinically relevant (Mehta & Shamoo, 2020). *Nocardia* are usually opportunistic bacteria that often trigger pulmonary infections. They also frequently disseminate to other organs, the skin, joints or brain. Central nervous system infections are highly acute forms of nocardiosis, with a mortality rate that ranges from 40% to 80% (Cattaneo *et al.*, 2013; McNeil & Brown, 1994; Wilson, 2012). The incidence of *Nocardia* infections is rather low, but is certainly underestimated: the identification of *Nocardia* species has been impaired by technical aspects, as it is mainly based on gene sequencing. Powerful methods such as matrix-assisted laser desorption/ionization time-of-flight (MALDI-TOF) mass spectrometry (Hodille *et al.*, 2023) are likely to enable better identification and may help to reveal the true incidence of this emerging class of bacteria.

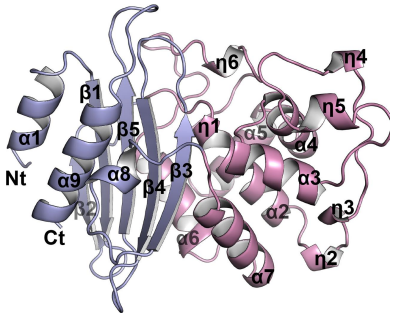

The reference treatment for nocardiosis, whatever the species, has long been based on a combination of two antibiotics, trimethoprim (TMP) and sulfamethoxazole (SMX), that target the folic acid pathway (Margalit *et al.*, 2021). Nonetheless, treating nocardiosis using this regimen remains very challenging and is often punctuated by treatment failure and/or relapse. This is mainly due to the high prevalence of strains that are drug-resistant to TMP–SMX (Uhde *et al.*, 2010). It is extremely difficult to treat disseminated forms of *Nocardia*, particularly those of the central nervous system. Treatment success is also impaired by difficulty in choosing and adapting the right drug regimen, since there is a large heterogeneity in drug susceptibility and drug resistance between the different human-pathogenic *Nocardia* species (Hershko *et al.*, 2023; Lebeaux *et al.*, 2019).

To circumvent these issues, the current recommendation is therefore a combination of different antibiotic classes. In addition to aminoglycosides and oxazolidinones, β-lactams are often used to treat nocardiosis. β-Lactam resistance has however been reported for *Nocardia*, with strong variations from one species to another. As stated in a retrospective study, while about 80% of *N. farcinica* strains are resistant to the β-lactam cefotaxime, only 5% of *N. cyriacigeorgica* strains are (Lebeaux *et al.*, 2019). β-Lactamases are enzymes that are capable of hydrolyzing β-lactam antibiotics and are classified into four classes according to the Ambler nomenclature (Ambler *et al.*, 1991; Bush, 2013). Classes A, C and D are serine hydrolases, while class B are metallo-β-lactamases that accommodate one or two zinc ions in their active site (Bahr *et al.*, 2021). It has not yet been fully documented whether *Nocardia* species possess all four β-lactamase classes; however, they certainly widely harbor class A β-lactamases (ABLs; Valdezate *et al.*, 2015). ABLs are usually capable of hydrolyzing a wide range of β-lactams and have been found, or can be found, in the genomes of most *Nocardia* species. Only four studies have described the biochemical characterization of these ABLs, notably those from *N. lactamdurans* (Coque *et al.*, 1993), *N. farcinica* (Laurent *et al.*, 1999; Lebeaux *et al.*, 2019) and *N. asteroides* (Poirel *et al.*, 2001).

To date, there is no report of any three-dimensional structure of an ABL from *Nocardia*. Such data could be helpful to fully reveal the differences in substrate specificity and inhibitor efficacy that are observed between ABLs from different *Nocardia* species (Laurent *et al.*, 1999; Lebeaux *et al.*, 2020; Poirel *et al.*, 2001). To fill this gap, in this study we describe the biochemical and structural characterization of an ABL from *N. cyriacigeorgica*, hereafter named NCY-1, which is one of the most commonly encountered human-pathogenic *Nocardia* species and for which β-lactam resistance has been reported (Zhao *et al.*, 2017).

2. Materials and methods

2.1. Gene amplification and cloning

Genomic DNA extracted from an *N. cyriacigeorgica* clinical isolate responsible for pulmonary nocardiosis was used as a template for polymerase chain reaction (PCR) with the primers 5′-GATATGCACCACGGCCTGCA-3′ and 5′-ACG GCGACGAAGAAGCGGA-3′ using Invitrogen Platinum SuperFi II DNA Polymerase (Thermo Fisher Scientific, Illkirch, France). A second PCR was performed on the abovementioned amplicon to amplify the truncated version of *NCY-1* using the following primers: forward, 5′-GGTACC GAGAACCTGTACTTCCAGGGTTCGGCCGTGGCCGA TCCCCGGTTCGCCGCACTGGAAACG-3′; reverse, 5′-GT GGTGCTCGAGCTAACCGAGCACGTCGACGACCGTC CTGGTCGCGTCGGC-3′. The purified PCR product was treated with DreamTaq polymerase (Thermo Fisher Scientific, Illkirch, France) to add an overhanging A at the 3′ end and cloned into Champion pET-SUMO (Invitrogen) following the manufacturer's instructions; correct insertion of the DNA fragment was verified by sequencing.

2.2. Protein expression and purification

The pET-SUMO::*NCY-1* plasmid was transformed into an *Escherichia coli* BL21 strain resistant to phage T1 (New England Biolabs) harboring the pRARE2 plasmid and plated onto LB+Agar plates supplemented with 50 µg ml^{-1} kanamycin and 30 µg ml^{-1} chloramphenicol. An overnight preculture was used to inoculate two flasks each containing 3 l LB with kanamycin and chloramphenicol. When the cells reached the exponential phase, they were placed on ice for 40 min and protein expression was induced with 1 m*M* isopropyl β-D-1-thiogalactopyranoside; the culture was then placed at 18°C overnight. The cells were harvested by centrifugation for 15 min at 6 000*g* and resuspended in 80 ml 50 m*M* Tris pH 8, 0.4 *M* NaCl, 5 m*M* β-mercaptoethanol, 1 m*M* benzamidine, 10% glycerol, 20 m*M* imidazole. The bacteria were lysed by sonication and centrifuged for 40 min at 27 000*g*. The clarified extract was loaded onto three gravity columns each containing 2 ml Ni–NTA Sepharose beads (Cytiva) at 4°C. The columns were then washed with 25 ml 50 m*M* Tris pH 8, 1 *M* NaCl, 5 m*M* β-mercaptoethanol, 10% glycerol and the proteins were eluted using a total of 30 ml buffer consisting of 50 m*M* Tris pH 8, 0.2 *M* NaCl, 5 m*M* β-mercaptoethanol, 10% glycerol, 200 m*M* imidazole. At this stage, about 230 mg of protein was recovered and the tag was cleaved by adding 4 mg of Tobacco etch virus (TEV) protease in a dialysis bag and dialyzing overnight at 4°C against 50 m*M* Tris pH 8, 0.2 *M* NaCl, 5 m*M* β-mercaptoethanol, 10% glycerol. A second nickel-affinity chromatography step was performed to separate the cleaved NCY-1 from the tags and the His-tagged TEV protease. To do so, two columns, each with 3 ml of beads, were equilibrated with dialysis buffer and the samples were loaded three times. The columns were washed with 20 ml dialysis buffer and 25 ml 50 m*M* Tris pH 8, 1 *M* NaCl, 5 m*M* β-mercaptoethanol, 10% glycerol. About 200 mg of NCY-1 was recovered in the flowthrough and the first wash step, concentrated to 5 mg ml^{-1} and flash-frozen in liquid nitrogen. For biochemical and crystallization purposes the protein was further purified by size-exclusion chromatography (SEC) on a Superdex 75 Increase 10/300 GL column

Table 1
Macromolecule-production information.

Source organism	*N. cyriacigeorgica* clinical strain
DNA source	Genomic DNA from *N. cyriacigeorgica* clinical strain
Forward primer for cloning into the expression vector	5′-GGTACCGAGAACCTGTACTTCCAGGGT TCGGCCGTGGCCGATCCCCGGTTCGCC GCACTGGAAACG-3′
Reverse primer for cloning into the expression vector	5′-GTGGTGCTCGAGCTAACCGAGCACGTC GACGACCGTCCTGGTCGCGTCGGC-3′
Cloning and expression vector	Champion pET-SUMO
Complete amino-acid sequence of the open reading frame	MRLAAAGARYWPRRSPRWCPSAVTSPASS FRRPGGRRMLAAALALSALAMTAACDS GSTTTAPATSAVTTSAVADPRFAALET TAGARLGVFAVNTGSERTVAHRADERF PMASTFKGLACGALLREHPLSTGYFDQ VIHYSAEELVDYSPVTETRVESGMTVA ELCHAAITASDNTAGNQLLKLLGGPQG FTAFLRSLGDDTSRLDRWETELNTAIP GDERDTTTPAALAADYRALVVGDVLGE PERAQLTAWLVANTTGDTRIRAGLPED WTVGDKTGSPAYGSALDVAVTWPSGRA PIVIAVLSTKSEQDAEPDNRLVADATR TVVDVLG
Complete amino-acid sequence of the construct expressed	MGSSHHHHHHGSGLVPRGSASMSDSEVNQ EAKPEVKPEVKPETHINLKVSDGSSEI FFKIKKTTPLRRLMEAFAKRQGKEMDS LRFLYDGIRIQADQTPEDLDMEDNDII EAHREQIGGGTENLYFQGSAVADPRFA ALETTAGARLGVFAVNTGSERTVAHRA DERFPMASTFKGLACGALLREHPLSTG YFDQVIHYSAEELVDYSPVTETRVESG MTVAELCHAAITASDNTAGNQLLKLLG GPQGFTAFLRSLGDDTSRLDRWETELN TAIPGDERDTTTPAALAADYRALVVGD VLGEPERAQLTAWLVANTTGDTRIRAG LPEDWTVGDKTGSPAYGSALDVAVTWP SGRAPIVIAVLSTKSEQDAEPDNRLVA DATRTVVDVLG
Complete amino-acid sequence of the construct after tag removal	GSAVADPRFAALETTAGARLGVFAVNTGS ERTVAHRADERFPMASTFKGLACGALL REHPLSTGYFDQVIHYSAEELVDYSPV TETRVESGMTVAELCHAAITASDNTAG NQLLKLLGGPQGFTAFLRSLGDDTSRL DRWETELNTAIPGDERDTTTPAALAAD YRALVVGDVLGEPERAQLTAWLVANTT GDTRIRAGLPEDWTVGDKTGSPAYGSA LDVAVTWPSGRAPIVIAVLSTKSEQDA EPDNRLVADATRTVVDVLG

(Cytiva); 5 mg of protein was injected and was eluted with buffer consisting of 20 m*M* Tris pH 8, 0.2 *M* NaCl, 0.5 m*M* *β*-mercaptoethanol, 5% glycerol. Macromolecule-production information is summarized in Table 1.

2.3. Assessment of the oligomeric state of NCY-1

A calibration curve was obtained using a Superdex 75 Increase 10/300 GL column with a total volume (V_t) of 23.56 ml connected to an ÄKTA Go (Cytiva). The proteins were eluted in 20 m*M* Tris pH 8, 0.2 *M* NaCl, 0.5 m*M* *β*-mercaptoethanol. A mixture of 600 µg bovine serum albumin, 200 µg carbonic anhydrase from bovine erythrocytes, 190 µg cytochrome *c* from horse heart and 400 µg bovine aprotinin were injected simultaneously and eluted at a flow rate of 0.3 ml min^{-1}. 300 µg of NCY-1 was injected independently and 400 µg of thyroglobulin was used to determine the void volume V_o. The volume of injection for each sample was 500 µl. The partition coefficient of each protein K_{av} was determined as follows: $K_{av} = (V_t - V_o)/(V_e - V_o)$, where V_e indicates the volume of elution of each protein. The calibration curve was obtained by plotting K_{av} against the logarithm of the molecular weight (MW).

Table 2
Crystallization.

Method	Vapor diffusion in sitting drops
Plate type	Swissci 48-well MRC MAXI Optimization Plates
Temperature (K)	291
Protein concentration (mg ml^{-1})	14
Buffer composition of protein solution	20 m*M* Tris–HCl pH 8, 0.2 *M* NaCl, 0.5 m*M* *β*-mercaptoethanol, 5% glycerol
Composition of reservoir solution	0.1 *M* citric acid, 10% PEG 6000, 6% ethylene glycol
Volume of the drop	1 µl + 1 µl
Reservoir solution (µl)	200

2.4. Crystallization

Crystals were obtained in sitting drops using a Swissci MRC MAXI plate, mixing 1 µl protein solution concentrated to 14 mg ml^{-1} with 1 µl reservoir solution consisting of 0.1 *M* citric acid pH 3.5, 10% PEG 6000, 6% ethylene glycol and equilibrating against a reservoir volume of 200 µl at 18°C. The crystals were cryoprotected by the addition of 4 µl of a solution consisting of 0.1 *M* citric acid pH 3.5, 14% PEG 6000, 20% ethylene glycol on top of the crystallization drop and incubated for 16 h before being cryocooled in liquid nitrogen. Crystallization information is summarized in Table 2.

2.5. X-ray data collection, structure determination and refinement

Data collection was performed on the PXI-X06SA beamline at the Swiss Light Source, Paul Scherrer Institut, Villigen, Switzerland. A total of 800 images were collected with an oscillation range of 0.2°, a crystal-to-detector distance of 145 mm and an X-ray wavelength of 0.9999 Å. Data were processed and scaled with the *XDS* package (Kabsch, 2010). The phase problem was solved by molecular replacement using *Phaser* (McCoy, 2007) and the *Phenix* package (Liebschner *et al.*, 2019), with an *AlphaFold* model (Jumper *et al.*, 2021) of NCY-1 as a search template. The structure was further manually rebuilt with *Coot* (Casañal *et al.*, 2020) and refined with the *Phenix* package (Liebschner *et al.*, 2019). The statistical values given in Tables 3 and 4 were calculated with *AIMLESS* from the *CCP*4 suite (Agirre *et al.*, 2023) and *Phenix* (Liebschner *et al.*, 2019).

2.6. Activity assays

The *β*-lactamase assay was performed in 96-well plates with a reaction volume of 100 µl in 1× phosphate-buffered saline (PBS) pH 7 in the presence of 0.2 m*M* nitrocefin. Reactions were initiated by the addition of 2, 4 or 8 n*M* enzyme or 8 n*M* enzyme incubated with 500 µ*M* avibactam for 30 min. A control reaction was performed with all components except the enzyme. The optical density at 486 nm was recorded for

Table 3
Data-collection statistics.

Values in parentheses are for the highest resolution shell.

Beamline	PXI-X06SA, SLS
Wavelength (Å)	0.9999
Data-collection temperature (K)	100
Resolution range (Å)	43.95–1.25 (1.28–1.25)
Space group	$P3_221$
a, b, c (Å)	54.18, 54.18, 131.86
α, β, γ (°)	90, 90, 120
Solvent content (%)	38.48
Total reflections	542218 (27178)
Unique reflections	63063 (3101)
Multiplicity	8.6 (8.8)
Completeness (%)	100 (100)
Mean $I/\sigma(I)$	12 (1)
Wilson B factor (Å^2)	17.7
R_{meas} (%)	7.8 (238.6)
$CC_{1/2}$	0.99 (0.28)

Table 4
Refinement statistics.

Values in parentheses are for the highest resolution shell.

PDB code	8qnn
Reflections used in refinement	62994 (4461)
Reflections used for R_{free}	2002 (141)
R_{work} (%)	14.16 (25.46)
R_{free} (%)	17.47 (30.42)
No. of non-H atoms	
Total	2196
Protein atoms	1960
Citrate atoms	26
Water molecules	210
Protein residues	259
R.m.s.d., bond lengths (Å)	0.007
R.m.s.d., bond angles (°)	0.936
R.m.s.d., planar groups (Å)	0.010
R.m.s.d., chiral centers (Å^3)	0.074
E.s.d. on atomic positions (Å)	0.14
Ramachandran favored (%)	97.28
Ramachandran allowed (%)	2.72
Ramachandran outliers (%)	0.00
Rotamer outliers (%)	0.00
Clashscore	1.79
Average B factor (Å^2)	
Overall	22.54
Protein	21.24
Citrate	25.75
Water molecules	34.28

75 min with data points acquired every 1 min using a Tecan Infinite 200 PRO M Plex plate reader.

3. Results and discussion

3.1. Gene amplification, construct design and protein expression

We first tried to amplify a β-lactamase gene from a *N. cyriacigeorgica* clinical strain using primers based on the sequence of the *N. cyriacigeorgica* GUH-2 chromosome complete genome (GenBank FO082843.1). This set of primers led to the amplification of a DNA fragment encompassing the β-lactamase AST-1 precursor (GenBank CCF63029.1). We then analyzed the putative open reading frame resulting from this nucleotide sequence and used *BLAST* to assess the sequence conservation. The final nucleotide sequence was deposited in NCBI GenBank under accession OR515607.

The translation of the nucleotide indicates an open reading frame (ORF) of 333 amino acids. As ABLs are synthesized as a precursor in the cytoplasm and then secreted into the periplasm (Kaderabkova *et al.*, 2022), we explored the possibility of the presence of a peptide signal. We analyzed the sequence with the *SignalP* server (Teufel *et al.*, 2022), which enabled us to identify a probable secretion signal with a cleavage site between Ala53 and Cys54. To further design an optimal sequence for protein expression and crystallization, we generated a predictive three-dimensional model with *AlphaFold* (Jumper *et al.*, 2021) to identify flexible/nonfolded regions. This analysis prompted us to design an ORF ranging from Ser71 to Gly333.

Finally, following this design approach, we cloned the nucleotide sequence of NCY-1 into an expression vector enabling fusion with a SUMO tag at the N-terminus as well as a multihistidine tag. We also added a sequence encoding the Tobacco etch virus protease between the tag and the coding sequence in order to remove the tag during the purification process. This strategy led to the production of a highly soluble form of NCY-1; following a two-step purification procedure, we could purify about 200 mg of protein from 6 l of culture using two nickel-affinity chromatography steps. The protein was further purified by SEC, leading to very pure and homogeneous protein, as shown in Fig. 1(*a*).

3.2. Protein quality assessment

To ensure that our construct-design strategy was successful and led to a well folded and functional protein, we first assessed the behavior of the protein on SEC. The calibration curve showed that NCY-1 behaves as a homogeneous and stable monomer with an apparent molecular weight of about 29 kDa, as expected from the theoretical molecular weight and for this class of enzymes, which are known to exist as monomers (Fig. 1*a*). We also conducted a β-lactamase activity assay. To do so, we used nitrocefin, a chromogenic cephalosporin substrate that shifts from a yellow to a red color upon β-lactamase activity. The presence of nanomolar concentrations of pure NCY-1 triggered the color shift shown in Fig. 1(*b*). The absorbance-monitoring assay showed increased absorbance at 486 nm in a NCY-1 concentration-dependent manner, in contrast to the two control experiments performed without enzyme or with enzyme incubated with avibactam, a covalent inhibitor of β-lactamases. Together, these data confirm that the construct design was successful and led to the production of a functional protein.

3.3. Crystallization, data collection and structure determination

We initiated the first crystallization trials at two different protein concentrations: 5 and 20.9 mg ml^{-1}. Most drops were clear, indicating that the protein was very soluble. Nonetheless, several conditions promoted the appearance of NCY-1 crystals. The best crystals were optimized in sitting drops at a protein concentration of 14 mg ml^{-1} and using a reservoir

solution consisting of 0.1 *M* citric acid pH 3.5, 10% PEG 6000, 6% ethylene glycol.

A full X-ray data set was collected and processed to a resolution of 1.25 Å (Table 3). The structure was solved by molecular replacement using the predicted model mentioned above as a search model. We finally rebuilt and refined the model to R_{work} and R_{free} values of 14.16% and 17.47%, respectively, with good geometry (Table 4). The asymmetric unit contained one monomer. Most of the residues could be rebuilt except for residues 71–73 and the glycine at the N-terminus from the TEV cleavage site. The last Gly333 at the C-terminus could also not be seen. In addition, we unambiguously identified two molecules of citrate that were present in the crystallization conditions. One of the citrate molecules is

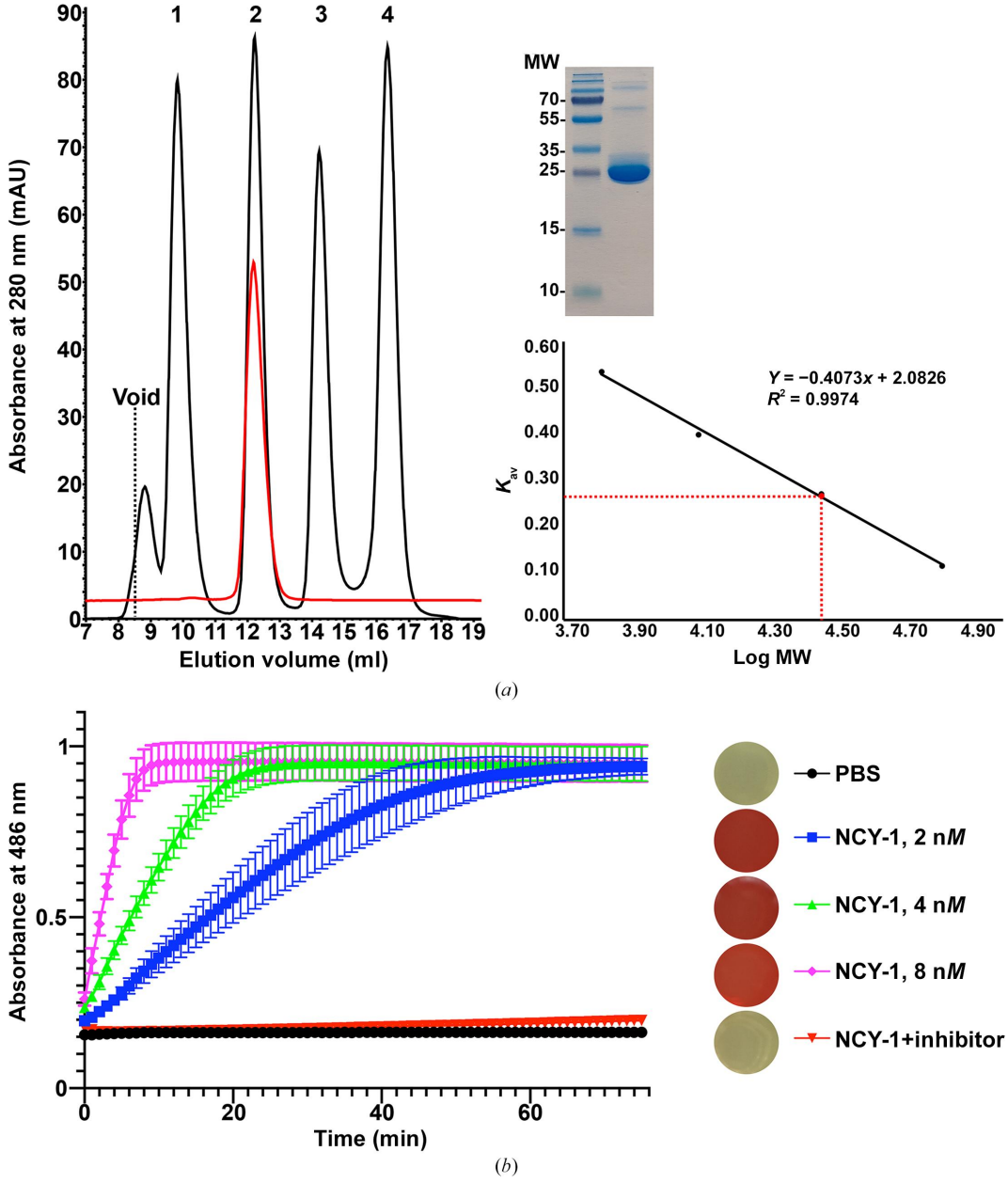

Figure 1
Evaluation of protein quality. (*a*) Size-exclusion chromatography profile of NCY-1 on a Superdex 75 Increase 10/300 GL column. The elution profile was compared with protein standards: bovine serum albumin (66 kDa, V_e = 9.82 ml), bovine carbonic anhydrase (29 kDa, V_e = 12.22 ml), horse cytochrome *c* (12.9 kDa, V_e = 14.22 ml) and bovine aprotinin (6.5 kDa, V_e = 16.33 ml). V_e indicates the elution volume. NCY-1 eluted at a volume of 12.18 ml. The void volume (V_o) was determined at 8.53 ml as the volume of elution of thyroglobulin (669 kDa). The NCY-1 (10 µg loaded) sample used for biochemical and structural analysis is shown on a 15% Coomassie-stained denaturing gel. (*b*) Determination of the *β*-lactamase activity of NCY-1 in the presence of nitrocefin. Three concentrations of the enzyme were tested (2 n*M*, blue curve; 4 n*M*, green curve; 8 n*M*, pink curve) and two control experiments were performed: the reaction background (black curve) performed with PBS instead of enzyme and the reaction with avibactam (red curve), a potent covalent inhibitor of *β*-lactamases. The data from three technical replicates were analyzed with *GraphPad Prism* version 10.0.2. On the right of the curves, pictures taken at the end of the reaction for each well are shown attesting to the color shift from yellow to red upon enzymatic reaction.

situated on the symmetry axis on the surface of the protein and contributes to the crystal packing of symmetry-related NCY-1 monomers and through interactions with Ala164, Glu165, His168, Gln250 and Trp254 (not shown). The second citrate is found in the active site and its interactions are described further below.

3.4. Structural analysis

NCY-1 has a classical ABL structure with an α/β-hydrolase fold comprised of two domains (Fig. 2*a*). The first domain is a mixed α/β-fold consisting of strands $\beta1$–$\beta5$ and helices $\alpha1$, $\alpha8$ and $\alpha9$. The second domain is fully α-helical and is formed by helices $\alpha2$, $\alpha3$, $\alpha4$, $\alpha5$, $\alpha6$ and $\alpha7$ (Fig. 2*a*). The structure is

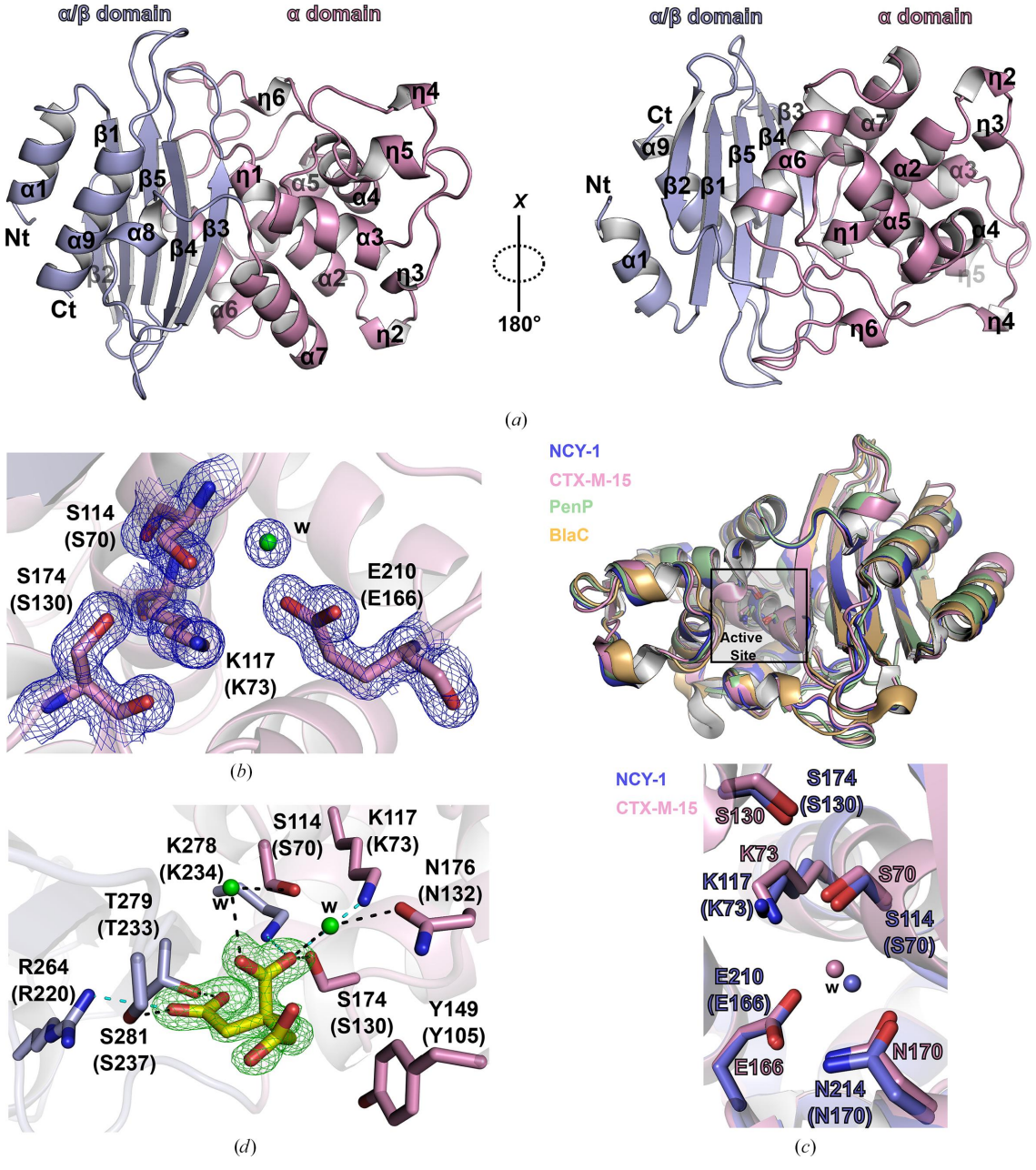

Figure 2
Structural analysis of NCY-1. (*a*) Cartoon representation of the three-dimensional structure of NCY-1 in two different orientations. The α/β domain is in blue and the α domain is in pink. Nt and Ct stand for N-terminus and C-terminus, respectively. (*b*) Depiction of important residues for the catalysis of class A β-lactamase activity. The $2F_o - F_c$ map (blue mesh) contoured at a level of 1σ shows the high quality of the electron-density map. W indicates a water molecule, which is displayed as a green sphere. Residues in parentheses indicate Ambler numbering. (*c*) Structural comparison of NCY-1 (blue) with its closest ABL homologues: PenP from *B. licheniformis* (green), CTX-M-15 (pink) and BlaC from *M. tuberculosis* (orange). The lower panel displays a close-up of the active sites of CTX-M-15 (pink) and NCY-1 (blue) and shows the strict conservation of catalytically important residues, which are shown as sticks, and water molecules (w). (*d*) The network of interactions between the citrate molecule and NCY-1 residues. Dashed black and cyan lines indicate hydrogen bonds and salt bridges, respectively. N atoms are colored in blue and O atoms are in red. The interactions were analyzed with the *PLIP* server (Adasme *et al.*, 2021). The simulated-annealing omit map proving the presence of the citrate is shown as yellow sticks. The map is contoured at a level of 3.5σ and is represented as a green mesh.

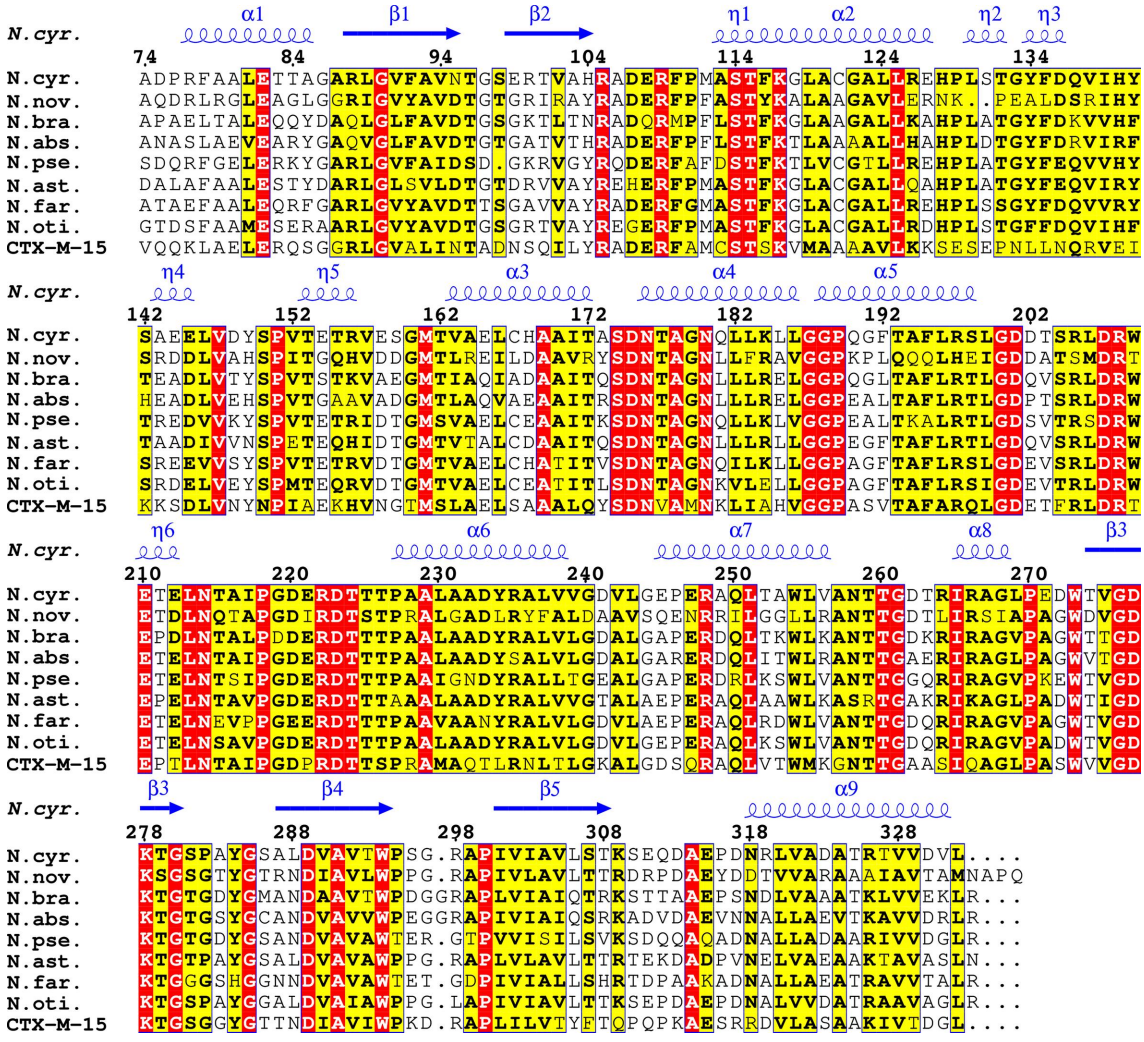

Figure 3
Multiple sequence alignment of class A β-lactamases from human-pathogenic *Nocardia*. The sequence of NCY-1 (N. cyr.) was aligned with the sequences of the ABLs from *N. otitidiscaviarum* NEB252 (N. oti.), *N. farcinica* IFM 10152 (N. far.), *N. brasiliensis* ATCC 700358 (N. bra.), *N. asteroides* NCTC11293 (N. ast.), *Nocardia nova* SH22a (N. nov.), *N. pseudobrasiliensis* ATCC 51512 (N. pse.) and *N. abscessus* NBRC 100374 (N. abs.), and CTX-M-15. The alignment displays only the sequences matching the NCY-1 residues that were modeled in the structure; thus, some of the sequences are missing some residues in the N-terminus. The secondary-structure elements from the NCY-1 structure are placed above the sequence alignment, where α, β and η indicate α-helix, β-sheet and 3_{10}-helix, respectively. The figure was generated with the *ENDscript* server (Robert & Gouet, 2014; https://endscript.ibcp.fr).

comprised of nine α-helices and six 3_{10}-helices. Five β-strands (β1–β5) form one antiparallel β-sheet and complete the structure. For clarity, and to match the standard nomenclature of ABLs, the residues indicated in parentheses follow the Ambler numbering scheme for ABLs (Ambler *et al.*, 1991).

In contrast to some other ABLs, we did not notice any disulfide bridges, although the Cys121 (Cys77) and Cys167 (Cys123) side chains on helices α2 and α3 are in close proximity. The absence of a disulfide bridge could be the result of the recombinant expression of the protein in the cytoplasm of *E. coli*, as we removed the secretion signal of NCY-1. The cytoplasm is indeed less favorable for the formation of disulfide bonds than the periplasm, where oxidative conditions are found and where β-lactamases are normally located.

The active-site residues and the water molecules in their proximity are well ordered and well defined in the electron-density map (Fig. 2*b*). The catalytic amino acids are at the interface of the two domains and are composed of Ser114 (Ser70), Lys117 (Lys73), Ser174 (Ser130) and Glu210 (Glu166) (Fig. 2*b*). These amino acids are strictly conserved when compared with other ABL structures from other phylae and particularly the well characterized CTX-M-15 (Figs. 2*c* and 3), in which these residues were shown to be crucial for hydrolysis of the β-lactam moiety (Tooke *et al.*, 2019).

Further analysis shows that the ABL sequence signature (Philippon *et al.*, 2019) is conserved, notably in the three motifs 114-STFK-117 (70-STFK-73), 174-SDN-176 (130-SDN-132) and 278-KTG-280 (234-KTG-236) (Fig. 3). The Glu210 (Glu166) residue on the so-called Ω-loop, which is important for ABL enzymatic activity, is also conserved. A detailed classification of β-lactamases based on multiple sequence alignment showed that subclass A1 (Philippon *et al.*, 2019)

possesses a clear signature sequence that presents, in addition to the three motifs mentioned above, 18 additional conserved residues. NCY-1 harbors strict conservation of these consensus residues (Fig. 3) as listed: Arg105 (Arg61), Arg109 (Arg65), Thr115 (Thr71), Gly122 (Gly78), Ala169 (Ala125), Asn180 (Asn136), Asp201 (Asp157), Arg208 (Arg164), Asn214 (Asn170), Asp223 (Asp179), Thr224 (Thr180), Thr225 (Thr181), Thr226 (Thr182), Pro227 (Pro183), Trp254 (Trp210), Arg266 (Arg222), Trp273 (Trp229) and Asp277 (Asp233).

We searched for the closest structures to NCY-1 in the entire Protein Data Bank using the *PDBeFold* server (https://www.ebi.ac.uk/msd-srv/ssm/ssmstart.html; Krissinel & Henrick, 2004). Because of the large number of ABLs for which structures have been determined, we retrieved numerous similar structures with an r.m.s.d. below 1 Å. The closest structure was the ABL from *Bacillus licheniformis* (PDB entry 1i2s; Fonzé *et al.*, 2002) named PenP, with an r.m.s.d. of 0.7 Å and 45% protein sequence identity. More interestingly, there was a close similarity (r.m.s.d. of 0.78 Å and 46% protein sequence identity) to the extended-spectrum β-lactamase CTX-M-15 from *E. coli* (PDB entry 4hbt; Lahiri *et al.*, 2013; Fig. 2*c*). We also found that an ABL from a species of the same order as *Nocardia*, namely BlaC from *Mycobacterium tuberculosis* (PDB entry 2gdn; Wang *et al.*, 2006), was slightly more distant, with an r.m.s.d. of 1 Å and 50% sequence identity. Further, a comparison of the active site of NCY-1 with that of the canonical CTX-M-15 demonstrates the strict conservation of key and important amino acids for catalysis, as well as identical positioning of the water molecule crucial for hydrolysis of the β-lactam ring (Fig. 2*c*). This analysis therefore suggests that NCY-1 might have a broad-spectrum substrate specificity like its closest homologues.

Additionally, we could unambiguously identify one citrate molecule that is tightly bound in the vicinity of the active site and is supported by the simulated-annealing $F_o - F_c$ omit map (Fig. 2*d*). The side chain of Tyr149 (Tyr105) interacts through van der Waals interactions (Fig. 2*d*). A network of hydrogen bonds between the side chains of Ser114 (Ser70), Ser174 (Ser130), Thr279 (Thr235) and Ser281 (Ser237) allows interaction with the citrate molecule, while Ser114 (Ser70) and Asn176 (Asn132) mediate specific interactions via water molecules. The tight binding of citrate is achieved by salt bridges involving Lys117 (Lys73), Arg264 (Arg220) and Lys278 (Lys234) (Fig. 2*d*). A similar interaction with citrate was previously observed for the structure of TEM-72, a class A β-lactamase from Enterobacteriaceae (Docquier *et al.*, 2011).

Finally, to address whether the NCY-1 structure is representative of ABLs from other *Nocardia* species, we performed a multiple sequence alignment of the ABLs from some of the most frequently encountered human-pathogenic *Nocardia* spp. (Fig. 3). This sequence analysis demonstrates a close conservation and sequence identity of NCY-1 with the ABLs from *N. nova* (49%), *N. brasiliensis* (66%), *N. abscessus* (65%), *N. pseudobrasiliensis* (65%), *N. asteroides* (69%), *N. farcinica* (72%) and *N. otitidiscaviarum* (77%), and with CTX-M-15 (45%). All of the proteins from *Nocardia* spp. have an almost strict conservation of the three motifs described earlier and the 18 residues characterizing class A1. Only a few substitutions were noticed in the class A1 signature in *N. abscessus*, *N. asteroides* and *N. nova*, but these probably had no consequence for the enzyme function as they do not concern residues that are critical for the activity of ABL (Tooke *et al.*, 2019). Thus, this analysis strongly suggests that all ABLs from pathogenic *Nocardia* species are likely to have very similar structures and that all of these species may possess functional ABLs, as it has already been shown for *N. farcinica* and *N. asteroides* (Laurent *et al.*, 1999; Poirel *et al.*, 2001).

Acknowledgements

We thank the CNRS, the IRIM directory and Dr K. Brodolin for support. We acknowledge the Paul Scherrer Institute, Villigen, Switzerland for the provision of synchrotron-radiation beamtime at beamline PXI-X06SA of the SLS. We thank Dr B. Iorga for fruitful discussions.

Funding information

JC's PhD fellowship is financed by the CNRS.

References

Adasme, M. F., Linnemann, K. L., Bolz, S. N., Kaiser, F., Salentin, S., Haupt, V. J. & Schroeder, M. (2021). *Nucleic Acids Res.* **49**, W530–W534.

Agirre, J., Atanasova, M., Bagdonas, H., Ballard, C. B., Baslé, A., Beilsten-Edmands, J., Borges, R. J., Brown, D. G., Burgos-Mármol, J. J., Berrisford, J. M., Bond, P. S., Caballero, I., Catapano, L., Chojnowski, G., Cook, A. G., Cowtan, K. D., Croll, T. I., Debreczeni, J. É., Devenish, N. E., Dodson, E. J., Drevon, T. R., Emsley, P., Evans, G., Evans, P. R., Fando, M., Foadi, J., Fuentes-Montero, L., Garman, E. F., Gerstel, M., Gildea, R. J., Hatti, K., Hekkelman, M. L., Heuser, P., Hoh, S. W., Hough, M. A., Jenkins, H. T., Jiménez, E., Joosten, R. P., Keegan, R. M., Keep, N., Krissinel, E. B., Kolenko, P., Kovalevskiy, O., Lamzin, V. S., Lawson, D. M., Lebedev, A. A., Leslie, A. G. W., Lohkamp, B., Long, F., Malý, M., McCoy, A. J., McNicholas, S. J., Medina, A., Millán, C., Murray, J. W., Murshudov, G. N., Nicholls, R. A., Noble, M. E. M., Oeffner, R., Pannu, N. S., Parkhurst, J. M., Pearce, N., Pereira, J., Perrakis, A., Powell, H. R., Read, R. J., Rigden, D. J., Rochira, W., Sammito, M., Sánchez Rodríguez, F., Sheldrick, G. M., Shelley, K. L., Simkovic, F., Simpkin, A. J., Skubak, P., Sobolev, E., Steiner, R. A., Stevenson, K., Tews, I., Thomas, J. M. H., Thorn, A., Valls, J. T., Uski, V., Usón, I., Vagin, A., Velankar, S., Vollmar, M., Walden, H., Waterman, D., Wilson, K. S., Winn, M. D., Winter, G., Wojdyr, M. & Yamashita, K. (2023). *Acta Cryst.* D**79**, 449–461.

Ambler, R. P., Coulson, A. F., Frère, J.-M., Ghuysen, J.-M., Joris, B., Forsman, M., Levesque, R. C., Tiraby, G. & Waley, S. G. (1991). *Biochem. J.* **276**, 269–270.

Bahr, G., González, L. J. & Vila, A. J. (2021). *Chem. Rev.* **121**, 7957–8094.

Bush, K. (2013). *J. Infect. Chemother.* **19**, 549–559.

Casañal, A., Lohkamp, B. & Emsley, P. (2020). *Protein Sci.* **29**, 1069–1078.

Cattaneo, C., Antoniazzi, F., Caira, M., Castagnola, C., Delia, M., Tumbarello, M., Rossi, G. & Pagano, L. (2013). *Int. J. Infect. Dis.* **17**, e610–e614.

Coque, J. J., Liras, P. & Martín, J. F. (1993). *EMBO J.* **12**, 631–639.

Docquier, J.-D., Benvenuti, M., Calderone, V., Rossolini, G.-M. & Mangani, S. (2011). *Acta Cryst.* F**67**, 303–306.
Fonzé, E., Vanhove, M., Dive, G., Sauvage, E., Frère, J.-M. & Charlier, P. (2002). *Biochemistry*, **41**, 1877–1885.
Hershko, Y., Levytskyi, K., Rannon, E., Assous, M. V., Ken-Dror, S., Amit, S., Ben-Zvi, H., Sagi, O., Schwartz, O., Sorek, N., Szwarcwort, M., Barkan, D., Burstein, D. & Adler, A. (2023). *J. Antimicrob. Chemother.* **78**, 2306–2314.
Hodille, E., Prudhomme, C., Dumitrescu, O., Benito, Y., Dauwalder, O. & Lina, G. (2023). *Int. J. Mol. Sci.* **24**, 5469.
Jumper, J., Evans, R., Pritzel, A., Green, T., Figurnov, M., Ronneberger, O., Tunyasuvunakool, K., Bates, R., Žídek, A., Potapenko, A., Bridgland, A., Meyer, C., Kohl, S. A. A., Ballard, A. J., Cowie, A., Romera-Paredes, B., Nikolov, S., Jain, R., Adler, J., Back, T., Petersen, S., Reiman, D., Clancy, E., Zielinski, M., Steinegger, M., Pacholska, M., Berghammer, T., Bodenstein, S., Silver, D., Vinyals, O., Senior, A. W., Kavukcuoglu, K., Kohli, P. & Hassabis, D. (2021). *Nature*, **596**, 583–589.
Kabsch, W. (2010). *Acta Cryst.* D**66**, 125–132.
Kaderabkova, N., Bharathwaj, M., Furniss, R. C. D., Gonzalez, D., Palmer, T. & Mavridou, D. A. I. (2022). *Microbiology*, **168**, 001217.
Krissinel, E. & Henrick, K. (2004). *Acta Cryst.* D**60**, 2256–2268.
Lahiri, S. D., Mangani, S., Durand-Reville, T., Benvenuti, M., De Luca, F., Sanyal, G. & Docquier, J.-D. (2013). *Antimicrob. Agents Chemother.* **57**, 2496–2505.
Laurent, F., Poirel, L., Naas, T., Chaibi, E. B., Labia, R., Boiron, P. & Nordmann, P. (1999). *Antimicrob. Agents Chemother.* **43**, 1644–1650.
Lebeaux, D., Bergeron, E., Berthet, J., Djadi-Prat, J., Mouniée, D., Boiron, P., Lortholary, O. & Rodriguez-Nava, V. (2019). *Clin. Microbiol. Infect.* **25**, 489–495.
Lebeaux, D., Ourghanlian, C., Dorchène, D., Soroka, D., Edoo, Z., Compain, F. & Arthur, M. (2020). *Antimicrob. Agents Chemother.* **64**, e01551–19.
Liebschner, D., Afonine, P. V., Baker, M. L., Bunkóczi, G., Chen, V. B., Croll, T. I., Hintze, B., Hung, L.-W., Jain, S., McCoy, A. J., Moriarty, N. W., Oeffner, R. D., Poon, B. K., Prisant, M. G., Read, R. J., Richardson, J. S., Richardson, D. C., Sammito, M. D., Sobolev, O. V., Stockwell, D. H., Terwilliger, T. C., Urzhumtsev, A. G., Videau, L. L., Williams, C. J. & Adams, P. D. (2019). *Acta Cryst.* D**75**, 861–877.
Margalit, I., Lebeaux, D., Tishler, O., Goldberg, E., Bishara, J., Yahav, D. & Coussement, J. (2021). *Clin. Microbiol. Infect.* **27**, 550–558.
McCoy, A. J. (2007). *Acta Cryst.* D**63**, 32–41.
McNeil, M. M. & Brown, J. M. (1994). *Clin. Microbiol. Rev.* **7**, 357–417.
Mehta, H. H. & Shamoo, Y. (2020). *PLoS Pathog.* **16**, e1008280.
Philippon, A., Jacquier, H., Ruppé, E. & Labia, R. (2019). *Curr. Res. Transl. Med.* **67**, 115–122.
Poirel, L., Laurent, F., Naas, T., Labia, R., Boiron, P. & Nordmann, P. (2001). *Antimicrob. Agents Chemother.* **45**, 878–882.
Robert, X. & Gouet, P. (2014). *Nucleic Acids Res.* **42**, W320–W324.
Teufel, F., Almagro Armenteros, J. J., Johansen, A. R., Gíslason, M. H., Pihl, S. I., Tsirigos, K. D., Winther, O., Brunak, S., von Heijne, G. & Nielsen, H. (2022). *Nat. Biotechnol.* **40**, 1023–1025.
Tooke, C. L., Hinchliffe, P., Bragginton, E. C., Colenso, C. K., Hirvonen, V. H. A., Takebayashi, Y. & Spencer, J. (2019). *J. Mol. Biol.* **431**, 3472–3500.
Uhde, K. B., Pathak, S., McCullum, I., Jannat-Khah, D. P., Shadomy, S. V., Dykewicz, C. A., Clark, T. A., Smith, T. L. & Brown, J. M. (2010). *Clin. Infect. Dis.* **51**, 1445–1448.
Valdezate, S., Garrido, N., Carrasco, G., Villalón, P., Medina-Pascual, M. J. & Saéz-Nieto, J. A. (2015). *Front. Microbiol.* **6**, 376.
Wang, F., Cassidy, C. & Sacchettini, J. C. (2006). *Antimicrob. Agents Chemother.* **50**, 2762–2771.
Wilson, J. W. (2012). *Mayo Clin. Proc.* **87**, 403–407.
Zhao, P., Zhang, X., Du, P., Li, G., Li, L. & Li, Z. (2017). *Sci. Rep.* **7**, 43660.